Investigation on the mechanism for crushing root-stubble and disturbing soil by bionic cutters and multi-curved cutters based on DEM

Chenggong Xie, Shunchang Guo, Yunpeng Gao, Xin Feng*,
Jiayue Yao, Yue Qin, Bendi Qi, Jingyu Hao
(*College of Engineering, Northeast Agricultural University, Harbin 150030, China*)

Abstract: In this study, to address the challenges of root-stubble crushed insufficiently and excessive disturbance of the soil on ridges, moving and fixed cutters imitating a cat's claw were designed for crushing stubble efficiently through reverse engineering technology. The multi-curve cutter was designed based on the distribution characteristics of roots in different soil layers, enabling efficient crushing of roots with minimal soil disruption. The EDEM was employed to build a root-stubble-soil discrete element model and simulate the crushing process of root-stubble. The accuracy of the result of the numerical simulation was validated through the field test. The qualified rate of root-stubble length, the rate of soil disturbance, and the power consumption of the device (PCD) would be increased with the increase of the rotational speed of cutter shaft (RSCS). The stubble, driven by the moving cutters, rotated around its root until a cutting support was established between the moving and fixed cutters, enabling efficient fragmentation. At a lower RSCS, the disturbed soil in the surface layer would fall back to the ridge. The soil in the middle and deep layers would also be collided and compressed by the soil in the surface layer, and a low rate of soil disturbance would occur. When the RSCS was 380 r/min, the rate of soil disturbance was the lowest, at 18.57%, and the qualified rate of root-stubble length could reach 91.07%, which could meet the requirements of agricultural technology.
Keywords: discrete element method, root-stubble treatment, soil protection, bionic cutter, multi-curve cutter
DOI: 10.25165/j.ijabe.20261902.10209

Citation: Xie C G, Guo S C, Gao Y P, Feng X, Yao J Y, Qin Y, et al. Investigation on the mechanism for crushing root-stubble and disturbing soil by bionic cutters and multi-curved cutters based on DEM. Int J Agric & Biol Eng, 2026; 19(2): 193–202.

1 Introduction

Soil is a precious natural resource, but it has suffered from severe erosion due to factors such as wind and water erosion, as well as improper tillage management[1,2]. Conservation tillage is crucial for soil protection through enhancing the resistance of soil to wind and water erosion through no-till and reduced-till practices. Root-stubble treatment is the key link before no-tillage and less-tillage sowing in conservation tillage[3]. Certain problems, such as the seeder blocked by root-stubble and the seeds contacted with stubble, would be caused by an improper root-stubble treatment[4-6]. The root-stubble includes both the stubble above the ground and the roots under the ground. The roots fix the soil, forming the soil-roots combination, which is challenging for mechanized treatment. Therefore, devices for crushing root-stubble need to be innovated, and such devices have been extensively studied by experts.

Wang et al.[7] proposed a vertical rotation-based straw strip cleaning and soil tillage method, and the performance of the designed device was evaluated by employing DEM-MFBD. Jia et al.[8], inspired by the saw-tooth structure and occlusion movement of locust mouth-parts, designed a device with a double bionic disc, and the rates of crushing straw and root-stubble were improved. Huang et al.[9] combined the technology of crushing stubble actively and guiding grass passively to innovate the device, and the performance of the device crushing and throwing stubble could be enhanced. Hou et al.[6] designed a lateral cutter to clean the stubble for no-tillage sowing, and proved through a field test that the new cutter could meet the requirements. He et al.[10] designed a vertical device for splitting maize stubble based on a crank slider mechanism, which improved the rate of crushing maize stubble. Lin et al.[11,12] designed an offset saw-tooth-disc based on the Archimedes line type, and cooperated with the star-type cutter for cleaning stubble and straw on the ridge. The efficiency of the device was improved.

Zhao et al.[13] designed a follow-up and self-adjusting angle cutter. The angle of the cutter could be passively adjusted based on the different depths of root-stubble and soil. Jiang et al.[14] designed a double-disc device. The stubble could be efficiently crushed by the opposite rotation of the wedge-shaped passive disc and the active disc cutter. Wang et al.[15] designed a vertical anti-blocking device with the double-disc. The characteristics of disturbing the straw were analyzed based on DEM. Li et al.[16] arranged three arc-shaped knives in a spiral distribution, and cooperated with a blower to achieve the crushing and cleaning of maize stubble and straw on the ridge. Jiang et al.[17] optimized the blade curve and arrangement of the cutter, and significantly improved the rate of crushing stubble. The design of crushing stubble cutters has seen significant optimization and innovation through the selection of cutting edges, combination of different cutters, and the application of bionic technology.

The majority of existing studies on the crushing of root-stubble with moving-fixed cutters have focused on the form of cutter shafts

Received date: 2025-09-19 **Accepted date:** 2026-01-26
Biographies: Chenggong Xie, MS, research interest: agricultural machinery, Email: s240701008@neau.edu.cn; **Shunchang Guo**, MS, research interest: agricultural machinery, Email: s240702093@neau.edu.cn; **Yunpeng Gao**, PhD, research interest: agricultural machinery, Email: b210701001@neau.edu.cn; **Jiayue Yao**, BS, research interest: agricultural machinery, Email: a07220079@neau.edu.cn; **Yue Qin**, BS, research interest: agricultural machinery, Email: qinyue@neau.edu.cn; **Bendi Qi**, MS, research interest: intelligent agricultural machinery, Email: s240702098@neau.edu.cn; **Jingyu Hao**, BS, research interest: agricultural machinery, Email: a07240116@neau.edu.cn.
***Corresponding author: Xin Feng**, PhD, Lecturer, research interest: intelligent agricultural machinery. College of Engineering, Northeast Agricultural University, Harbin 150030, China. Tel: +86-13204656939, Email: fengxin@neau.edu.cn.

that rotate horizontally. There is a need for innovation in the cutter structure based on the form of cutter shafts that rotate vertically. Previous studies have demonstrated that the root-stubble could be efficiently crushed based on the method in which the cutter shaft rotates horizontally. However, this method can result in a high rate of soil disturbance when the cutter is used for crushing roots. In the context of ridge tillage and sowing, the original ridge structure could be compromised, increasing the complexity of ridge reconstruction and potentially leading to significant soil erosion. Consequently, the issue of soil disturbance caused by cutters during the root-stubble crushing process requires attention and further investigation to mitigate its environmental impact and ensure sustainable agricultural practices.

Biomimetics, as an interdisciplinary field, investigates the structural characteristics, locomotion principles, and functional mechanisms formed by organisms during long-term evolution in nature. By introducing biomimetic principles into the field of agricultural machinery and applying them to the optimized design of key components, it is possible to enhance operational performance, reduce energy consumption, and provide new approaches for the innovative development of agricultural machinery. Tong et al.[18] designed a biomimetic cutter for crushing stubble based on the geometrical structure of the toe tips of the mole rat, which improved the rate of crushing straw. Zhang et al.[19] designed a biomimetic cutter inspired by the fore claws of the nymph of cryptotympana atrata, which significantly improved the performance of crushing maize straw. He et al.[20] designed a biomimetic disc cutter for crushing wheat straw based on the claw structure of the mole, which effectively reduced the crushing resistance. Qi et al.[21] designed a biomimetic shearing device based on the multi-tooth structure of the leaf-cutting ant's mandibles and the unique bite mode of its mandibles, which increased the rate of shearing maize stubble and reduced shearing resistance.

In recent years, numerical simulation techniques have demonstrated significant advantages in the field of agricultural engineering. DEM is one of the numerical methods employed to predict the motion characteristics of particles[22,23]. It could clarify the relationship between agricultural particles and cutters. The development cost and design cycle of agricultural machinery could be shortened[24]. DEM has become a mature method employed to study the machine for conservation tillage[25]. For example, DEM was employed to investigate the effect of various edge curves on the torque of the cutter shaft and the characteristics of disturbing soil[26], analyzing the interactions among the furrow opener, straw, and soil[27].

The maize roots are closely bound to the soil, forming a root-soil complex, making it inefficient for traditional horizontal crushing devices to achieve effective fragmentation and simultaneously increasing soil disturbance during the crushing process. For conservation tillage, it is required to crush roots under a low disturbance of the soil. Bionic technology has been proven to improve the performance of crushing root-stubble and could be employed to innovate cutter structures[28]. In response to the above issues, in this study, the cutter imitating a cat's claw for crushing stubble and the cutter composed of different curves for crushing roots were designed. The cutters were integrated vertically to crush root-stubble simultaneously. The mechanism of crushing the root-stubble and disturbing the soil was revealed. The effect of operating parameters of the device with the new cutters on crushing stubble and disturbing soil was assessed through simulation and field experiment. This study demonstrated that the vertical cutter shaft configuration allows for the simultaneous and efficient crushing of roots and stubble under low power consumption, while effectively preserving the original ridge shape. The findings not only provide a technical basis for the structural design of devices of crushing root-stubble, but also propose a sustainable root-stubble management approach. The study offers an effective solution to a key challenge of balancing the improvement of the quality of crushing root-stubble with soil protection in conservation tillage.

2 Design of vertical crushing root-stubble device

2.1 Design of a bionic cutter inspired by cat's claw for crushing stubble

In previous field tests, during the operation of the vertical rotary crushing device, stubble tended to slip along the crushing edge of the moving cutter, escaping the overlapping range by the moving and fixed cutters, thereby adversely affecting the crushing effectiveness of the root-stubble. During the process of climbing or hunting activities, cats utilize a rotary motion driven by their tendon mechanisms, while their claw hook structure enables secure grasping of target surfaces[29,30]. By emulating these principles, the bionic cutter inspired by the cat's claw was optimized to effectively prevent slippage of root-stubble. This design prevented incomplete crushing caused by the stubble moving out of the crushing range, thereby ensuring thorough crushing of stubble. Inspired by the tearing function of a cat's claw on the prey, we selected the claw of a British Shorthair cat as our bionic prototype. The external contour of the cat's claw was observed under a microscope (OLYMPUS-SZX16), and the inner and outer contour curves of cat's claw were obtained through MATLAB software. The fitting equations of the inner and outer contours are shown in Equations (1) and (2). Based on these curves, the shape of the moving and fixed cutters imitating cat's claw were designed. The surface width of the maize ridge was 150 mm, and the moving cutters must have sufficient length to smoothly crush stubble. Its radius of rotation should not be less than the stubble growth range, so the length of the moving and fixed cutters was designed as 150 mm. According to the *Agricultural Machinery Design Handbook*, the overlap length between the moving and fixed cutters was designed as 120 mm. To meet agronomic requirements, the length of crushed stubble should not exceed 50 mm. Considering that operational vibration may cause relative positional variations between the moving and fixed cutters, the vertical clearance between them should not be excessively small and was determined to be 20 mm. Field measurements indicated that the height of stubble was 0-15 cm. To accommodate different heights of stubble while ensuring the operational stability of the cutter shaft, the shaft length was determined to be 210 mm, as shown in Figure 1[31].

$$f(x_1) = 16\sin(0.41x_1 - 0.60) + 14\sin(0.43x_1 + 2.46) \quad (R^2 = 0.997) \quad (1)$$

$$f(x_2) = 0.001\,64x_2^3 - 0.088\,56x_2^2 + 1.116x_2 + 0.3409 \quad (R^2 = 0.997) \quad (2)$$

By analyzing the characteristics of crushing roots at different soil depths and the effects of cutters on soil disturbance, and in combination with the distribution characteristics of roots, the soil was divided into three layers: 0-3 cm, 3-6 cm, and 6-9 cm. The 0-3 cm layer was the surface soil, which was a key layer for maintaining ridge structural stability and erosion resistance. The 3-6 cm layer contained a relatively concentrated distribution of roots and served as the primary zone for water and nutrient uptake and transport. The 6-9 cm layer exhibited a broader root distribution range, although the root density was relatively lower. Targeted crushing-edge designs were implemented for specific layers: The sinusoidal curve, characterized by its smooth soil penetration and minimal disturbance to soil structure, was employed to design the cutter edge for the 0-3 cm layer. The formula of the sinusoidal cutter edge curve is shown in Equation (3). For the 3-6 cm soil layer, an Archimedean spiral was employed to minimize soil disturbance and effectively crush root systems while generating a "root extraction" effect[24,32]. The formula of the Archimedean spiral cutter edge curve is shown in Equation (4). For the 6-9 cm soil layer, an involute curve was employed to achieve uniform force distribution during crushing roots, thus reducing energy consumption[33]. The formula of the involute cutter edge curve is shown in Equation (5). The design is shown in Figure 1. During this period, the action of the multi-curve cutter was sequenced according to the rotational radius, processing soil layers progressively from the largest to the smallest radius. The involute crushing edge had the largest rotational radius, first contacting the roots in the 6-9 cm soil layer. With a wide sweeping range and relatively uniform force distribution, it effectively severed the sparsely distributed deep roots while reducing disturbance to the deeper soil. As the cutter continued to rotate, the Archimedean spiral crushing edge acted on the more densely distributed roots in the 3-6 cm soil layer. While crushing the roots, this edge also provided guiding and pulling effects on the crushed roots, pulling them upward. The sinusoidal crushing edge had the smallest rotational radius and finally cut the roots in the 0-3 cm soil layer. Owing to its smooth penetration characteristics, the sinusoidal edge effectively minimized damage to the surface soil structure. The different crushing-edge designs, operating with a vertical rotary motion, achieved the coordination of crushing root-stubble and soil disturbance, thereby satisfying the low-disturbance requirements of conservation tillage[31].

$$y_3 = 9.52\sin(-0.62x_3) \quad (-0.52 < x_3 < 0) \tag{3}$$

$$\begin{cases} x_4 = 4.67(1+0.5t_4)\cos(t_4) - 3.41 \\ y_4 = 4.67(1+0.5t_4)\sin(t_4) + 1.48 \end{cases} \quad (-0.413 < t_4 < 0.3) \tag{4}$$

$$\begin{cases} x_5 = 6.11(\cos t_5 + t_5\sin t_5) + 4.4 \\ y_5 = 6.11(\sin t_5 - t_5\cos t_5) + 14.56 \end{cases} \quad (1.74 < t_5 < 2.28) \tag{5}$$

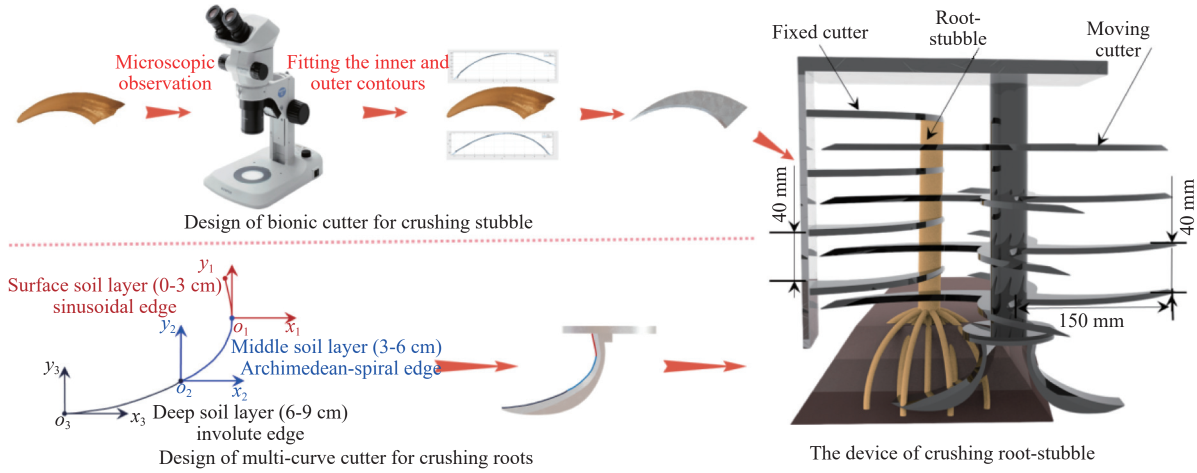

Figure 1 Design of cutters for crushing root-stubble

2.2 Basic parameters determination for roots, stubble and soil

The field test site was Harbin city, Heilongjiang Province (126°63′N, 45°75′E). Before the test, soil samples were collected from a 0-10 cm depth employing a ring cutter. These samples were then dried at 105°C for a duration of 24 h[34]. The soil moisture content and soil bulk density were (1.36±0.20) g/cm³ and 24.6%±0.5% (wet-based), respectively.

A Vernier caliper was employed to measure basic dimensions of the ridge platform. The height and diameter of stubble, the ridge spacing, and the plant spacing were (15.0±3.0) cm, (2.9±0.2) cm, (65.0±2.0) cm, and (26.0±0.3) cm, respectively. The moisture content of roots and stubble were 15.60%±0.80% and 23.23%±0.60%, respectively[35]. For the study, the necessary power for operating the device to crush the root-stubble was provided by a JD2C-354 tractor.

3 Methods

3.1 Numerical simulation method for root-stubble crushing

Based on measured root-stubble samples, a three-dimensional root-stubble model was established at a 1:1 scale using CATIA software, saved in STEP format, and imported into EDEM. To characterize the mechanical differences between stubble and root, the stubble and root were respectively filled with particles of physical radius of 2.0 mm and 1.5 mm in EDEM, and the "Hertz-Mindlin with bonding" contact model was selected to simulate the internal structural characteristics of the stubble and roots. A soil bin with a length of 1 m was constructed in EDEM. A ridge with height of 10 cm and upper and lower ridge widths of 15 cm and 30 cm, respectively, was established in the soil bin and filled with particles of physical radius of 1.5 mm. The "Hertz-Mindlin with JKR" contact model was employed to simulate the adhesive interactions among soil particles, between soil and roots, and between soil and the cutters of crushing roots. Previous studies have demonstrated that "Hertz-Mindlin with JKR" contact model could maintain the structural integrity of the root-soil complex by simulating the adhesion between roots and soil particles. The root-stubble crushing device was simplified and imported into EDEM. The basic operating parameters of the device were defined to analyze the mechanism of crushing root-stubble. The simulation model of crushing root-stubble and physical parameters of particles in the simulation are shown in Figure 2[36-41].

3.2 Design of simulation test

3.2.1 Test factors

The relationship between the forward speed (FS) of the power unit and the rotational speed of the cutter shaft (RSCS) was obtained through calibration, as listed in Table 1. Then, MATLAB software was employed to fit the relationship between FS and RSCS; the fitting equation is listed below.

$$y_6 = 225.92\ln^{x_6} + 458.39 \quad (R^2 = 0.978) \tag{6}$$

where, y_6 is RSCS, r/min; x_6 is FS, m/s.

Based on the Agricultural Machinery Design Handbook, the range of RSCS was 380-540 r/min, which was taken as the factor range in the single factor test. RSCS was inserted into Equation (6) to calculate the corresponding FS. Within the rotational speed range of 380-540 r/min, an excessive number of test levels might have minimized data variability and thereby obscured differences among results. Conversely, an excessively low level might have introduced excessive variability, adversely affecting the accuracy and reliability of the results. Based on a comprehensive analysis, five levels were selected[42,43]. The experimental results showed a clear trend of change across all five levels for each measured index, which supported the rationality of selecting these five levels. The single factor test was arranged (380 r/min, 0.71 m/s; 420 r/min, 0.84 m/s; 460 r/min, 1.01 m/s; 500 r/min, 1.20 m/s; 540 r/min, 1.43 m/s). Each group of simulation test was repeated three times.

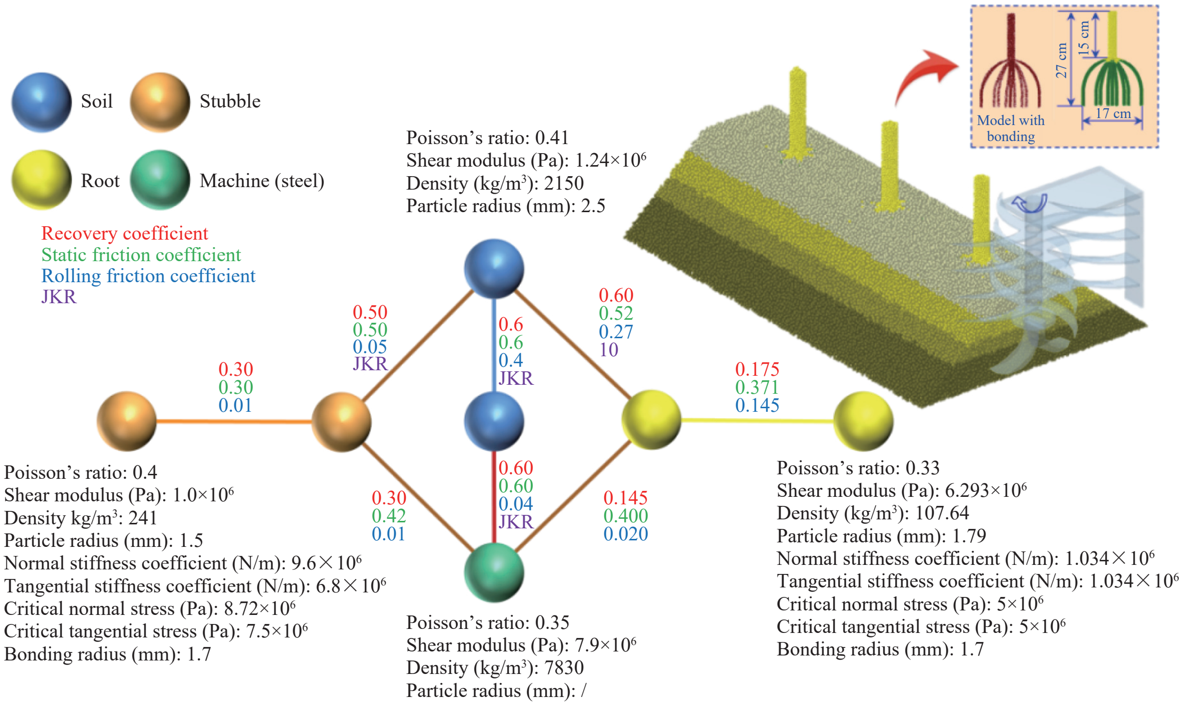

Figure 2 Simulation model of crushing root-stubble and physical parameters of particles in the simulation

Table 1 The relationship between FS and RSCS

Parameter	Value				
FS/m·s^{-1}	0.37	0.51	0.64	0.77	1.03
RSCS/r·min^{-1}	240	300	342	418	462

3.2.2 Test indicators

In the simulation test, the qualified rate of root-stubble was calculated as the proportion of particles meeting the crushing requirements relative to the total number of particles, specifically determined using Equation (7).

$$y_7 = \left(1 - \frac{S_2}{S_1}\right) \times 100\% \tag{7}$$

where, y_7 is the qualified rate of root-stubble length, %; S_1 is the average particle count of a single root-stubble before crushing; S_2 is the total particle count of a single root-stubble that fails to meet crushing requirements after the crushing.

To evaluate soil disturbance, taking the center of the first root-stubble as the starting point and the center of the second root-stubble as the ending point, the ridge within the crushing zone was equally divided into five segments along the forward travel direction of the machine. Then, the cross-sectional profiles of these five disturbed ridge platform segments, as well as the profile of the original undisturbed ridge platform, were extracted in EDEM software. MATLAB software was employed to calculate the cross-sectional area values for each profile. These area values were then substituted into Equation (8) to determine the soil disturbance.

$$y_8 = \frac{v_1 + v_2 + v_3 + v_4 + v_5}{5v_0} \times 100\% \tag{8}$$

where, y_8 is the rate of soil disturbance, %; v_1, v_2, v_3, v_4, v_5 are the five cross-sectional areas evenly divided in the ridge platform within a single root-stubble crushing area; v_0 is the original cross-sectional area of the ridge platform, cm^2.

The analysis module in EDEM was employed to obtain real-time torque of the cutter shaft during root-stubble crushing. The PCD was then determined through Equation (9).

$$y_9 = \frac{Tn}{9550} \times 100\% \tag{9}$$

where, y_9 is PCD, kW; T is the real-time torque of the cutter shaft, N/m; n is RSCS, r/min.

3.3 Design of field test

Before field test, five maize root-stubble were grouped as a set of test objects. To ensure accurate collection and analysis of the crushed stubble, they were sprayed and dyed as shown in Figure 3. Each group of tests was repeated five times.

Before field test, 15 root-stubbles were excavated and the adhering soil was cleaned off. The mass of these 15 root-stubble was measured using an electronic scale, and their average mass was calculated. Subsequently, during each replicate test, root-stubble which failed to meet the crushing standard were collected and weighed. Finally, the measured data were substituted into Equation (10) to calculate the qualified rate of root-stubble for the field test.

$$y_{10} = \left(1 - \frac{M_2}{5M_1}\right) \times 100\% \tag{10}$$

where, y_{10} is the qualified rate of root-stubble length, %; M_1 is the average quality of a single maize root-stubble before crushing, g; M_2 is the total quality of root-stubble failing to meet crushing requirements per group.

As shown in Figure 4c, when calculating the rate of soil disturbance, a single complete crushing process was taken as the object of analysis. The region between the centers of the two adjacent root-stubbles was defined as the start and end points, and the ridge within this region was equally divided into five segments along the forward travel direction of the device. Statistical analysis was then performed on the cross-sectional areas of soil of each segment. This region covered all operational stages of crushing roots, while the equally spaced cross sections reflected the spatial variation characteristics of soil disturbance. This approach also enabled consistent positioning between field and simulation tests, facilitating subsequent analysis of result consistency. The cross-sectional areas of both each disturbed segment and the original ridge were measured using a soil profiler[44]. These values were then substituted into Equation (8) to calculate the soil disturbance degree.

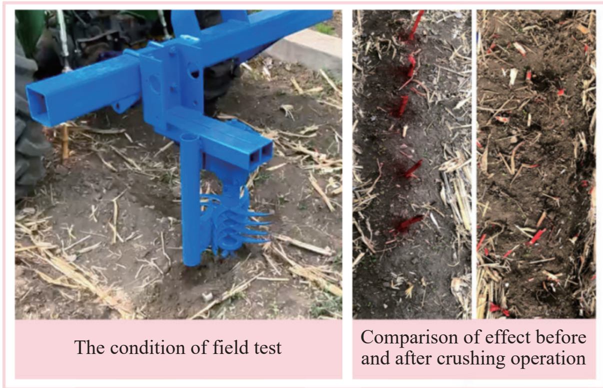

Figure 3 Field test condition and root-stubble crushing performance

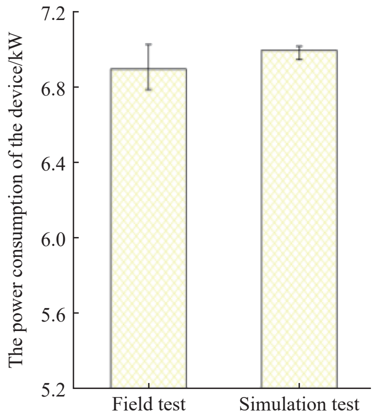

a. Power consumption of the device

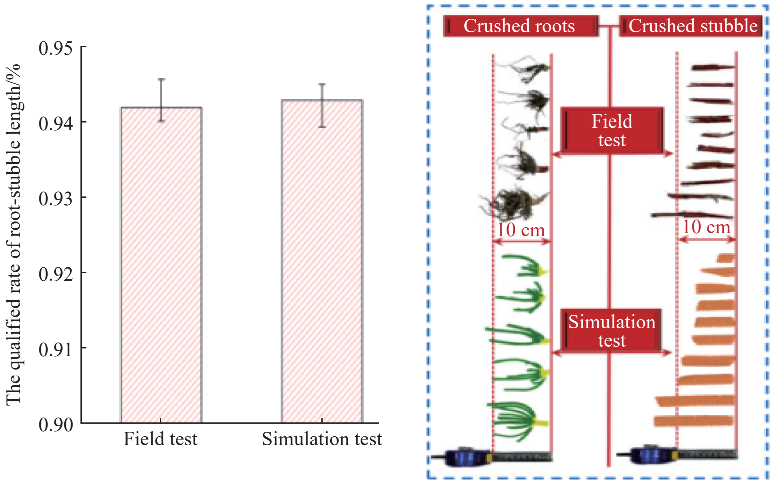

b. Qualified rate of root-stubble length

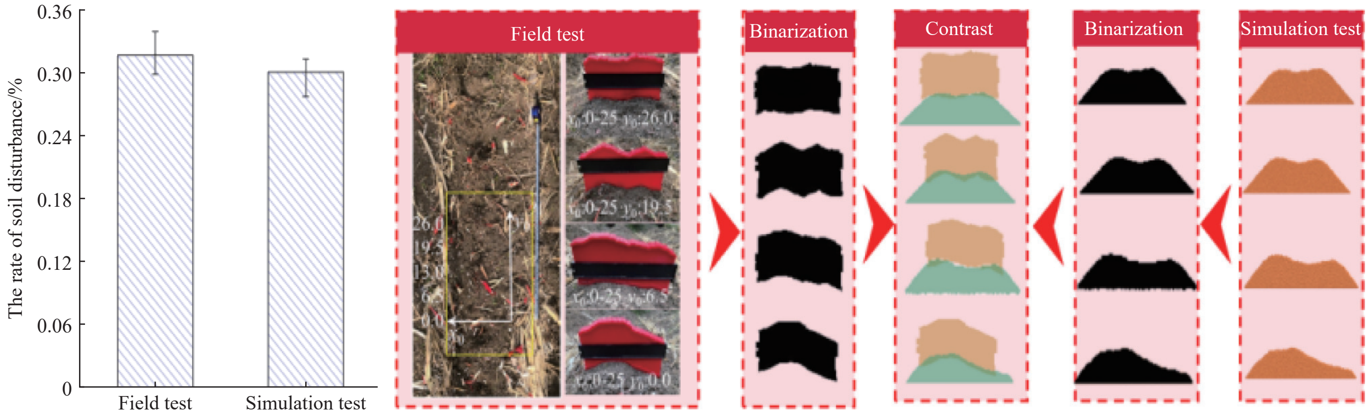

c. Rate of soil disturbance

Figure 4 Comparison of the results in the field and simulation tests

The torque measurement device primarily consists of external strain gauges (GC350-3HA) bonded to an elastic element, a signal processing module (Your cee-HX 711), a power supply, and connecting wires, as shown in Figure 3. The strain gauges output an electrical signal corresponding to the cutter shaft torque. This signal is amplified and digitized by the signal processing module before being transmitted to signal processing software. Prior to test, the torque measurement device was attached on the universal joint. During field test, the data acquisition software received and processed the digital signal from the signal processing module in real time to calculate the torque value of the cutter shaft. Then PCD was calculated through Equation (9).

4 Results and discussion

4.1 Consistency of the results in the field and simulation tests

The RSCS of 460 r/min, which was in the mid-range of the tested speeds (380-540 r/min), was selected as it represented the typical operating condition of the device. Under this condition, key performance indicators such as the qualified rate of crushing root-stubble, the rate of soil disturbance, and power consumption were all at moderate levels, demonstrating high representativeness. In field test with RSCS of 460 r/min, compared with the simulation test results under the corresponding conditions, the errors of PCD, the qualified rate of root-stubble length, and the rate of soil disturbance were 0.1 kW, 0.10%, and 1.59%, respectively. During the forward movement of the device, the involute crushing edge with the largest radius of rotation first acted on the deep soil layer, causing soil to be thrown from the center of the ridge toward both sides and forming an “M” shaped ridge at the initial stage of crushing roots. As the machine continues to advance, the Archimedean spiral crushing edge and the sinusoidal crushing edge successively disturbed the middle and surface soil layers. Within their respective action areas, the soil was thrown outward from the rotational center of the crushing shaft, ultimately forming a “Λ” shaped ridge at the final stage of crushing roots. The results of field test and simulation test showed that the ridge profiles after crushing root-stubble obtained from both tests were highly consistent, both exhibiting a transition from “M” to “Λ” configuration along the direction of device movement. This proved that the multi-curve cutter of crushing root-stubble effectively crushed maize root-stubble while maintaining the original ridge shape. Additionally, the high consistency between the shapes of crushed root-stubble and ridge, observed in simulations and field tests, further indicated that a root-soil complex similar to field conditions had been successfully formed in the DEM model. The results proved the high accuracy of using the “Hertz-Mindlin with JKR” contact model and the “Hertz-Mindlin with bonding” contact model to simulate the process of crushing root-stubble and the interaction between cutters and soil. The comparison results are shown in Figure 4.

4.2 Effect of RSCS on the qualified rate of root-stubble length

As shown in Figures 5a and 5b, during the process of crushing root-stubble, the stubble was contacted and gathered within the area

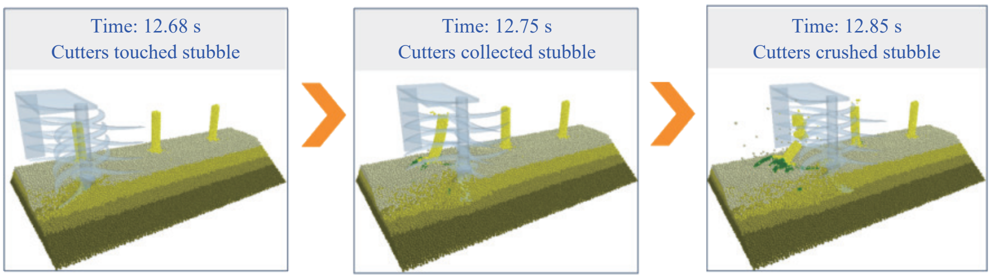

a. Process of crushing stubble

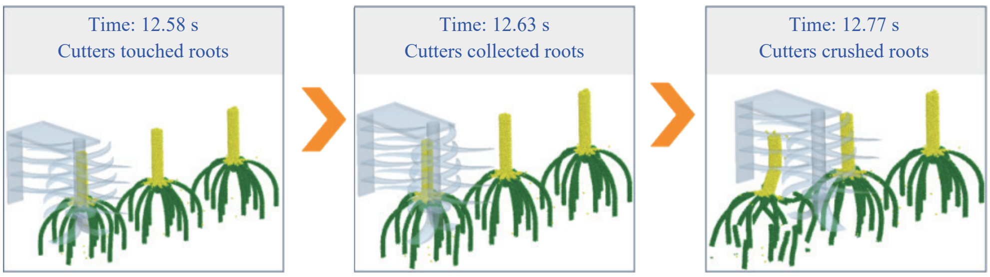

b. Process of crushing roots

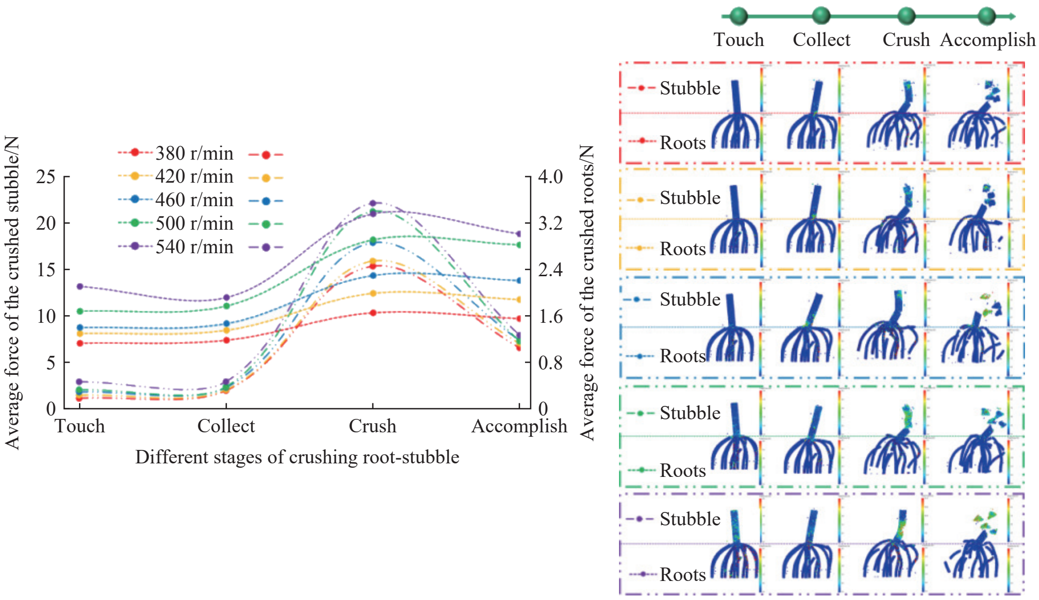

c. Effect of RSCS on average force of the crushed root-stubble

Figure 5 Crushing process of root-stubble of the fixed cutters by moving cutters. The stubble was crushed by support from the cooperation of moving and fixed cutters. During this period, the action of the multi-curve cutter was sequenced according to the rotational radius, processing soil layers progressively from the largest to the smallest radius. The involute crushing edge, which had the largest rotational radius, first crushed the widely distributed roots in the deep soil layer, ensuring stable penetration and uniform force distribution. Subsequently, the Archimedean spiral crushing edge operated in the middle soil layer, crushing the concentrated roots while simultaneously pulling the crushed roots upward. Finally, the sinusoidal crushing edge, with the smallest rotational radius, smoothly penetrated the shallow soil layer and crushed the main roots with minimal soil disturbance.

With the increase of RSCS, the qualified rate of root-stubble length increased. When RSCS was 380 r/min, the qualified rate of root-stubble length was the lowest, with a value of 91.07%. When RSCS was 540 r/min, the qualified rate of root-stubble length was the highest, and its value could reach 95.3%. This analysis indicates that as RSCS increases, the impact force exerted by the moving cutters on the root-stubble also increases, thereby enhancing the effectiveness of crushing root-stubble.

The process of crushing root-stubble could be divided into four distinct stages based on time: touching, collecting, crushing, and accomplishing, as shown in Figure 5c. When RSCS was 380 r/min, the average force exerted on the stubble in the touching stage was relatively low, with a value of 1.11 N. In the stage of collecting stubble, the stubble rotated around its roots due to the action of the moving cutters, resulting in only a slight increase in the force compared to that in the touching stage. In the crushing stage, the force reached its peak due to the support provided by the moving cutters to the stubble, increasing by 14.22 N compared to that in the touching stage. When crushing stubble was accomplished, the support from the moving and fixed cutters ceased, leading to a decrease in the average force exerted on the stubble. The force exerted on the roots at each stage was significantly lower than that on the stubble. This was primarily due to the smaller rotation radius of the cutter crushing roots, which resulted in a lower linear velocity at their tip and consequently less impact on the roots. Additionally, the presence of soil during the process of crushing roots further reduced the force exerted on the roots; however, it was still sufficient to crush the roots. As RSCS increased, the average force exerted on the root-stubble in each stage exhibited an upward trend. At RSCS of 540 r/min, the average force exerted on the root-stubble in the crushing stage reached 22.11 N, representing an increase of 7.89 N compared to that at RSCS of 380 r/min. This finding aligned with the results as shown in Figure 6.

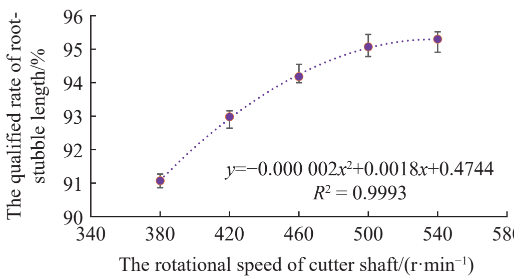

Figure 6 Effect of RSCS on the qualified rate of root-stubble length

4.3 Effect of RSCS on the rate of soil disturbance

The soil disturbance process could be divided into three distinct stages: initial contact with roots, crushing roots, and pulling roots. As shown in Figure 7, the surface soil exhibited higher velocities in the stages of initial contact with and pulling roots along the Z-axis (the direction in which the soil was thrown) compared to the other stage. This phenomenon would occur while the linear velocities at the contact points of the cutters were higher when the cutters contacted with the roots. Under the influence of rotating cutters, the soil experienced a more pronounced disturbance in the positive direction of the Z-axis. As the device moved forward, the tips of the cutters gradually lifted away from the soil, causing the contact point with the soil to shift from the tips to the ends of the cutters. Consequently, the disturbance effect of the cutters on the soil diminishes, leading to a decrease in the velocity of soil along the Z-axis. The disturbance effect of the cutters was most pronounced in the pulling process. This was because the crushed roots ejected outward by the cutters, and the entanglement between the roots and soil increased the velocity of the soil, thereby enhancing the soil disturbance. This phenomenon can be summarized as the high disturbance effect on the surface soil layer of the roots.

As RSCS increased, the velocity of the soil at the same stage within the same soil layer also increased. In the three stages, the velocity of the soil in the surface soil layer along the Z-axis exhibited relatively small variations. This indicated that the cutter with sinusoidal edge could penetrate the soil smoothly during vertical rotation. In the process of crushing the roots in the surface soil layer, the effect on the soil was uniform, resulting in relatively minor disturbance. In contrast, in the middle and deep soil layers, the soil displayed a consistent disturbance pattern. Different from the surface soil layer, where the motion of the soil was mainly affected by the cutters, those in the middle and deep layers were extruded by the surface soil layer. The linear velocity of the cutters was higher due to their larger radius of rotation. When roots were crushed, the soil in the area underwent significant displacement. The Archimedean spiral, involute curve, and the interactions among soil played a pivotal role in disturbing soil. As a result, the velocity of the soil in the middle and deep layers was relatively low, leading to a weaker disturbance, which was considered advantageous. Figure 7 clearly shows that the velocity of soil in the middle and deep layers was significantly lower than that in the surface layer.

With the increase of RSCS, the rate of soil disturbance increased. When RSCS reached 540 r/min, the rate of soil disturbance peaked at 35.34%, which was significantly higher than that at RSCS of 380 r/min. This phenomenon would be attributed to the increase of the linear velocity of the cutters, which enhanced the velocity of the soil in all soil layers, as shown in Figure 7. As illustrated in Figure 8, the distribution of the soil in different layers was also investigated. At lower RSCS, the velocity of the soil was minimal, resulting in the relatively small displacements of the soil. Consequently, most soil tended to fall back onto the ridge. This phenomenon was a key reason for the low rate of soil disturbance observed at lower RSCS. In the middle and deep soil layers, the surface soil layer exerted an obstruction effect that further decreased the already small displacement of the soil in these layers, thereby maximizing the preservation of the original state of the ridges. This constituted the second reason for the low rate of soil disturbance. When RSCS was higher, the initial velocity of soil would be higher, resulting in relatively larger displacements of the soil. Compared to low RSCS, more soil would fall into the furrow. The initial velocity of soil in the middle and deep soil layers also increased, further enhancing its displacement. Additionally, the weakening of the hindrance from the surface soil layer contributed to the increase in the rate of soil disturbance.

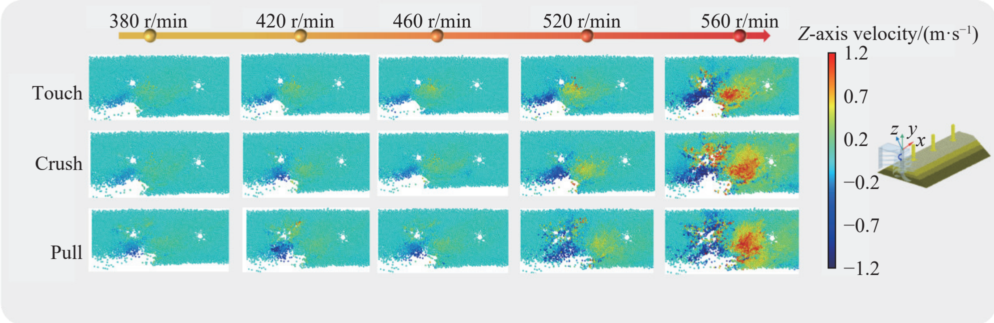

a. Surface soil layer (0-3 cm)

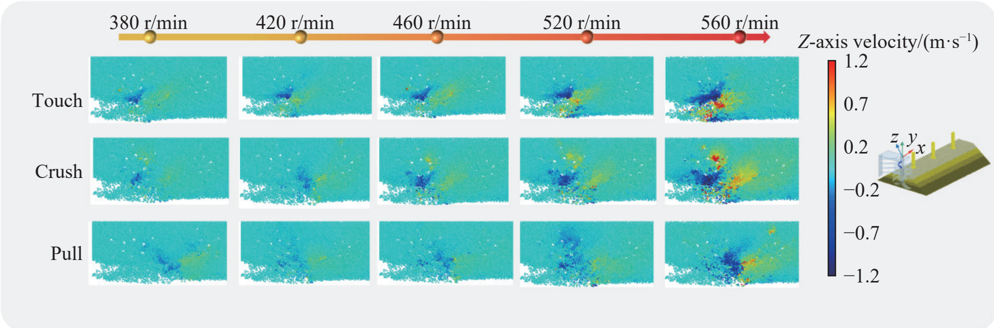

b. Surface soil layer (3-6 cm)

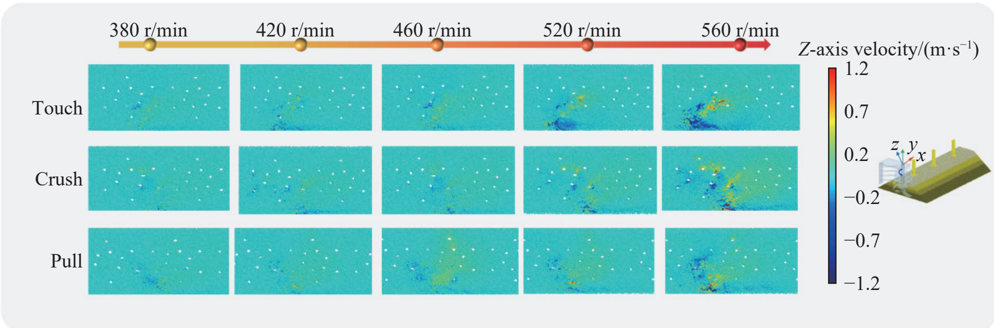

c. Surface soil layer (6-9 cm)

Figure 7 The disturbance of the soil

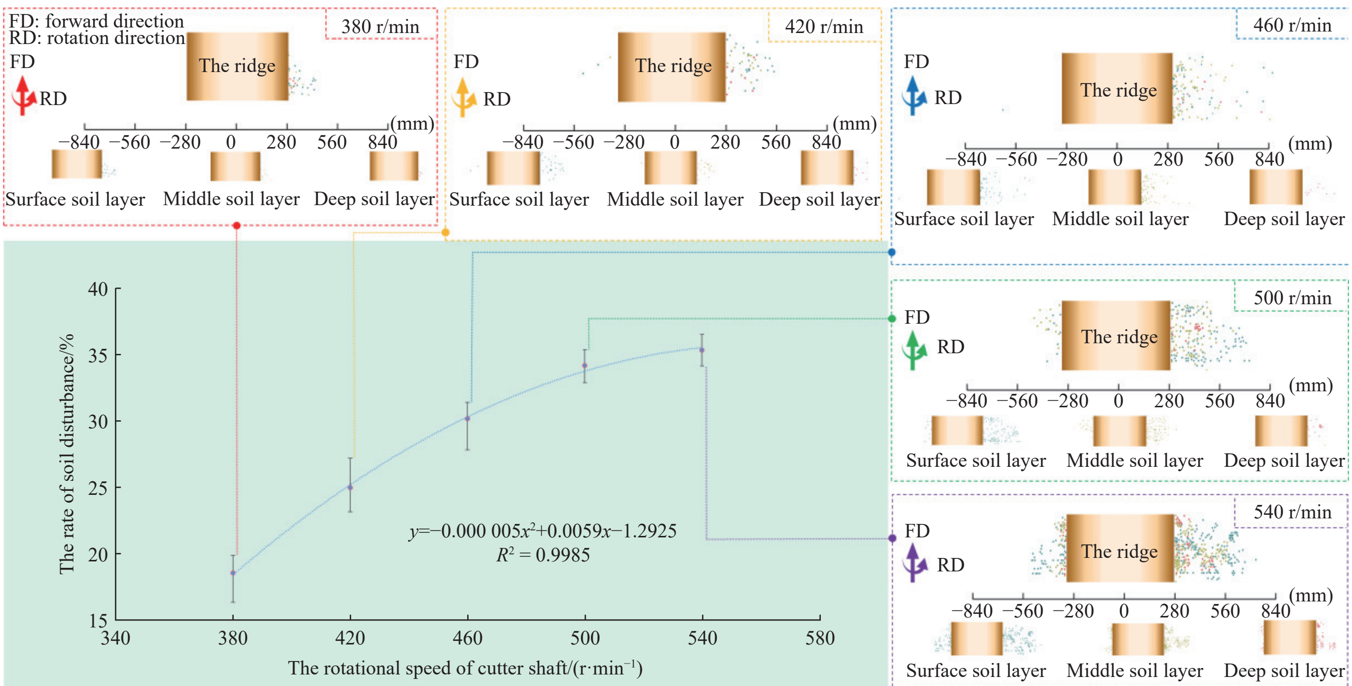

Figure 8 Effect of RSCS on the rate of soil disturbance

4.4 Effect of RSCS on PCD

As illustrated in Figure 9, PCD increased with the increase in RSCS, which aligned with the conclusions drawn by Vu et al.[45] When RSCS was 540 r/min, PCD was the largest, and its value was 8.1 kW. When RSCS was 380 r/min, PCD was the smallest, and its value was 4.1 kW. The higher the RSCS, the greater the kinetic energy of moving cutters. The increased energy was more conducive to crushing the root-stubble, which led to a higher qualified rate of root-stubble length. In the process of crushing root-stubble and disturbing the soil, the high RSCS corresponded to the high FS, and the area of cutter sweeping the soil would increase per unit time. Therefore, PCD would increase due to the energy required for crushing root-stubble and disturbing soil.

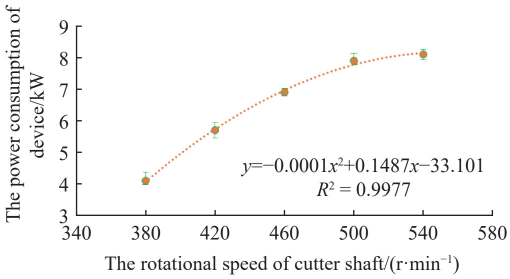

Figure 9 Effect of RSCS on PCD

5 Conclusions

In this study, inspired by the mechanics of a cat's claw, the cutter for crushing stubble above the ground was designed based on reverse engineering technology. The cutter composed of different curves was designed to crush roots under the ground based on the distribution characteristics of roots. The cutters were integrated vertically to crush root-stubble simultaneously. EDEM was employed to build a root-stubble-soil discrete element model and investigate the effect of the innovative device on crushing root-stubble and disturbing soil at different RSCS. Finally, field tests were conducted.

1) The simulation result for the qualified rate of root-stubble length was 94.28%, while the field test result was 94.18%. For PCD, the simulation result was 7.0 kW compared to the field test result of 6.9 kW. The errors were only 1% and 0.1 kW, respectively. This demonstrated the feasibility of using the "Bonding model and JKR" model to simulate the crushing of root-stubble. Furthermore, the simulation result for the rate of soil disturbance was 30.18%, closely matching the field test result of 31.77% with an error of only 1.59%. Additionally, after crushing, both the simulation results and field test results showed a transformation in ridge shape from "M" to "Λ", proving the accuracy of using the JKR model to simulate the interaction between the cutters and the soil.

2) The test shows that the bionic moving cutters effectively gathered stubble, preventing their slippage, and then cooperated with the bionic fixed cutters to achieve supportive cutting, effectively crushing stubble. Simultaneously, the different cutting-edge curves of multi-curve cutter were employed to sequentially carry, pull out, and crush root systems at varying depths. This approach not only ensured effective crushing of roots but also minimized soil disturbance. With the increase of RSCS from 380 to 540 r/min, the qualified rate of root-stubble length increased from 91.07% to 95.30%, the rate of soil disturbance increased from 18.57% to 35.34%, PCD increased from 4.1 to 8.1 kW, and all met the agricultural technical specifications.

3) The study reveals that when RSCS was 380 r/min, the cutters demonstrated exceptional performance for crushing root-stubble. The proportion of root-stubble meeting the required length specifications reached 91.07%, which significantly enhanced the decomposition efficiency of the crushed stubble and thereby promoted the cycling of organic matter within the soil-crop system. Under this operational parameter, the device demonstrated significant ecological benefits. The rate of soil disturbance was only 18.57%, which was significantly lower than that of conventional cutters. Additionally, the PCD was 4.1 kW. The device achieved crushing of root-stubble while maximally preserving the original ridge shape, effectively reducing soil disturbance and providing favorable seedbed conditions for subsequent sowing. In addition, the device could operate in coordination with supporting agricultural machinery, such as seeders, demonstrating high practical application value. However, the current investigation was mainly focused on the maize planting pattern of ridge tillage in Northeast China, and the adaptability of the device under other soil types and crop conditions has not been validated. To achieve low energy consumption and soil disturbance, the device needed to operate at relatively low forward speeds, which constrained field efficiency. Future studies should aim at further optimization and validation with respect to multi-crop and multi-soil adaptability, as well as improvements in operational efficiency.

Acknowledgements

This work was supported by the National Natural Science Foundation of China (Grant No. 52205253) and the Heilongjiang Provincial Natural Science Foundation (Youth Category B) Project (Grant No. YQ2025E001).

[References]

[1] Han X Z, Zhou W X. Research perspectives and footprint of utilization and protection of black soil in northeast China. Acta Pedologica Sinica, 2021; 58(6): 1341–1358. (in Chinese)

[2] Fang H Y. Impacts of rainfall and soil conservation measures on soil, SOC, and TN losses on slopes in the black soil region, Northeastern China. Ecological Indicators, 2021; 129: 108016.

[3] Feng X, Yao J Y, Gao Y P, Zeng L C, Wang L J, Wang B, et al. Review of root-stubble characteristics and root-stubble crushing and clearing technologies for conservation tillage. Sustainability, 2024; 16(19): 8508.

[4] Li X J, Wu J A, Zhao D Y, Zhang C L, Zhou F J. Research on straw pretreatment equipment of corn no-tillage planter. Journal of Chinese Agricultural Mechanization, 2021; 42(7): 1–7. (in Chinese)

[5] Jiang S, Wang Q J, Zhong G Y, Tong Z W, Wang X H, Xu J. Brief review of minimum or no-till seeders in China. AgriEngineering, 2021; 3(3): 605–621.

[6] Hou S Y, Zhu Y F, Zhu X X, Wang Y J, Ji W Y, Chen H T. Design and experiment of a straw clearing mulching no-tillage planter. Biosystems Engineering, 2022; 2221: 69–80.

[7] Chen G B, Wang Q J, Li H W, He J, Wang X H, Zhang X Y, et al. Experimental research on vertical straw cleaning and soil tillage device based on soil-straw composite model. Computers and Electronics in Agriculture, 2024; 216: 108510.

[8] Jia H L, Guo M Z, Gou C J, Zheng J, Zhang C L, Zhao J L. Design of dynamic bionic stubble cutting device and optimization test of parameters. Transactions of the CSAM, 2018; 49(10): 103–114. (in Chinese)

[9] Huang Y X, Gao P Y, Zhang Q K, Shen H, Zhu R X, Shi J T. Design and experiment of grass-soil separation device with combination of stubble cutting and grass guiding used for no-till planter. Transactions of the CSAM, 2020; 51(5): 67–78. (in Chinese)

[10] Lin H, He J, Li H W, Wang Q J, Lu C Y, Yang W C, et al. Design and experiment of a reciprocating intermittent chopping device for maize straw returning. Agriculture, 2022; 12(2): 220.

[11] Lin J, Li B, Li B, Niu J, Qian W. Parameter optimization and experiment on Archimedes spiral type of gap cutting disc. Transactions of the CSAM, 2014; 45(6): 118–124. (in Chinese)

[12] Lin J, Qian W, Niu J L. Design and experiment of stubble-cutting and anti-blocking mechanism for ridge-till and no-till planter. Journal of Shenyang Agricultural University, 2015; 46(6): 691–698. (in Chinese)

[13] Wang J Y, Zhao S H, Gao L L, Yuan Y W, Yang Y Q. Design and experiment of passive disc cutting blade in corn ridges. Transactions of the CSAM, 2021; 52(11): 59–67. (in Chinese)

[14] Jiang J L, Gong L N, Wang D W, Wang G P. Design and experiment for driving double coulters anti-blockage device of no-till planter. Transactions of the CSAE, 2012; 28(21): 17–22. (in Chinese)

[15] Wang W W, Zhu C X, Chen L Q, Li Z D, Huang X, Li J C. Design and experiment of active straw-removing anti-blocking device for maize no-tillage planter. Transactions of the CSAE, 2017; 33(24): 10–17. (in Chinese)

[16] Li X J, Zhang C L, Zhao D Y, Wu J A, Li Q D, Zhou F J. Design and experiment of air-sweeping type straw stubble processor. Journal of Chinese Agricultural Mechanization, 2021; 42(5): 13–18. (in Chinese)

[17] Jiang T J. Design and experimental study on gear-tooth stubble cutting mechanism of no-tillage seeder. Jilin University, 2013.

[18] Tong J, Ji W F, Jia H L, Chen D H, Yang X W. Design and tests of biomimetic blades for soil-rototilling and stubble-breaking. Journal of Bionic Engineering, 2015; 12: 495–503.

[19] Chang Z Y, Liu W, Tong J, Guo L, Xie H, Yang X, et al. Design and experiments of biomimetic stubble cutter. Journal of Bionic Engineering, 2016; 13: 335–343.

[20] Torotwa I, Ding Q S, Makange N R, Liang L, He R Y. Performance evaluation of a biomimetically designed disc for dense-straw mulched conservation tillage. Soil and Tillage Research, 2021; 212: 105068.

[21] Qi H Y, Ma Z C, Xu Z H, Wang S, Ma Y H, Wu S Y, et al. The design and experimental validation of a biomimetic stubble-cutting device inspired by a leaf-cutting ant's mandibles. Biomimetics, 2023; 8(7): 555.

[22] Fang W Q, Wang X Z, Han D L, Chen X G. Review of material parameter calibration method. Agriculture, 2022; 12(5): 706.

[23] Zhao J W, Yu J Q, Sun K, Wang Y, Liang L S, Sun Y C, et al. A discrete element method model and experimental verification for wheat root systems. Biosystems Engineering, 2024; 244: 146–165.

[24] Zhang S L, Huang Y X, Gao X J, Bi Y B, Dong J X, Zhao H B, et al. Evaluating the influence of straight-plain types of rotary tiller blades with various edge curves on maize residue using DEM. Biosystems Engineering, 2024; 250: 49–61.

[25] Wang J W, Xu Y N, Wang C Y, Xiang Y S, Tang H. Design and simulation of a trenching device for rice straw burial and trenching based on MBD-DEM. Computers and Electronics in Agriculture, 2023; 207: 107722.

[26] Zhao H B, Li H W, Ma S C, He J, Wang Q J, Lu C Y, et al. The effect of various edge-curve types of plain-straight blades for strip tillage seeding on torque and soil disturbance using DEM. Soil and Tillage Research, 2020; 202: 104674.

[27] Zhu D Q, Shi M H, Yu C Y, Yu Z Y, Kuang F M, Xiong W, et al. Tool-straw-paddy soil coupling model of mechanical rotary-tillage process based on DEM-FEM. Computers and Electronics in Agriculture, 2023; 215: 108410.

[28] Luo Y Q, Li J L, Yao B H, Luo Q, Zhu Z C, Wu W B. Research progress and development trend of bionic harvesting technology. Computers and Electronics in Agriculture, 2024; 222: 109013.

[29] Vollmerhaus B, Roos H. Die kralle der hauskatze (*Felis catus*)-eine formenanalyse. Anatomia Histologia Embryologia, 2000; 29: 193–195.

[30] Roos H, Vollmerhaus B. Konstruktionsprinzipien an der vorder- und hinterpfote der hauskatze (*Felis catus*). 4. Mitteilung: Muskelinnervation und bewegungsanalyse. Anatomia Histologia Embryologia, 2005; 34: 2–14.

[31] Feng X, Xie C, Tong J, Guo S, Qi B, Gao Y, et al. Design and test of vertical axis rotating cutters for cutting corn roots and crown. Agriculture, 2025; 15: 717.

[32] Lin J, Lyu Z, Li H, Wang X, Wang D. Design and experiment of passive anti-winding stubble breaking and ridge cleaning device for no-tillage planter. Transactions of the CSAM, 2023; 54(6): 19–27, 37. (in Chinese)

[33] Sun Y X, Dou G Z, Duan W B, Chen X H, Zheng J, Xin L M, et al. Involute-arc-leg for multi-legged robot: high stability and low energy consumption. Mechanism and Machine Theory, 2022; 170: 104701.

[34] Liu L, Wang X L, Zhang X C, Cheng X P, Wei Z C, Zhou H, et al. The impact of 'T'-shaped furrow opener of no-tillage seeder on straw and soil based on discrete element method. Computers and Electronics in Agriculture, 2023; 213: 108278.

[35] National Feed Quality Inspection Center, Feed quality inspection center of the ministry of agriculture. GB/T14699.1-2005, Feed Sampling. Beijing: China Standards Press, 2005.

[36] Tang Z Y, Gong H, Wu S L, Zeng Z W, Wang Z Q, Zhou Y H, et al. Modelling of paddy soil using the CFD-DEM coupling method. Soil and Tillage Research, 2023; 226: 105591.

[37] Zhang J, Xia M, Chen W, Yuan D, Wu C Y, Zhu J P. Simulation analysis and experiments for blade-soil-straw interaction under deep ploughing based on the discrete element method. Agriculture, 2023; 13(1): 136.

[38] Yuan Y W, Wang J Y, Zhang X, Zhao S H. Effect of rotary speed on soil and straw throwing process by stubble-crushing blade for strip tillage using DEM-CFD. Agriculture, 2023; 13(4): 877.

[39] Zhang S L, Zhao H B, Wang X Z, Dong J X, Zhao P F, Yang F F, et al. Discrete element modeling and shear properties of the maize stubble-soil complex. Computers and Electronics in Agriculture, 2023; 204: 107519.

[40] Wang Q, Wang Z M, Zhang Z H, Zhang K, Yao S, Zhou W Q, et al. Design and test of bionic elastic row cleaner with improved straw cleaning performance. Agriculture, 2024; 14(2): 186.

[41] Shi Y Y, Sun X, Wang X C, Hu Z C, Newman D, Ding W M. Numerical simulation and field tests of minimum-tillage planter with straw smashing and strip laying based on EDEM software. Computers and Electronics in Agriculture, 2019; 166: 105021.

[42] Hou S Y, Ji Z C, Xue D H, Wang X, Feng B J, Chen H T. Improved design and test of straw cleaning device suitable for no-tillage seeding unit. Transactions of the CSAM, 2023; 54(7): 111–122. (in Chinese)

[43] Xiao M H, Niu Y, Wang K X, Zhu Y J, Zhou J B, Ma R Q. Design of self-excited vibrating rotary tiller and analysis of its performance in reducing torsion and consumption. Transactions of the CSAM, 2022; 53(11): 52–63. (in Chinese)

[44] Hou S Y, Chen H T, Zou Z, Wei Z P, Zhang Y L. Design and test of lateral stubble cleaning blade for corn stubble field. Transactions of the CSAE, 2020; 36(2): 59–69. (in Chinese)

[45] Vu V D, Ngo Q H, Nguyen T T, Nguyen H C, Nguyenet Q T, Nguyen V D. Multi-objective optimization of cutting force and cutting power in chopping agricultural residues. Biosystems Engineering, 2020; 191: 107–115.